Received: 30 December 2025 | Accepted: 31 May 2026

DOI: 10.1002/hem3.70424

HemaSphere eha

ARTICLE

Passenger variants as pan-clonal markers of pediatric AML: Implications for molecular MRD

Ruth Shiloh[1,2,^] | Dana Dayan[3,4,^,] | Ifat Geron[1,2] | Maor Cohen[2,5] | Tamar Feuerstein[1] | Jorge Cano-Nistal[3,4] | Nurit Gal-Mark[1,2] | Shlomit Barzilai-Birenboim[1,6] | Dafna Gaash[1] | Michal Hameiri-Grossman[1] | Avraham Kahan[3,4] | Jamal Mahajna[5] | Nino Oniashvili[1] | Hava Rosenfeld[1] | Dan Scharf[3,4] | Keren Shichrur[1] | Elena Shinderman-Maman[1] | Sarah Elitzur[1,6] | Yehudit Birger[1,2,6] | Shai Izraeli[1,2,6,^] | Yosef E. Maruvka[3,4,^]

Graphical Abstract

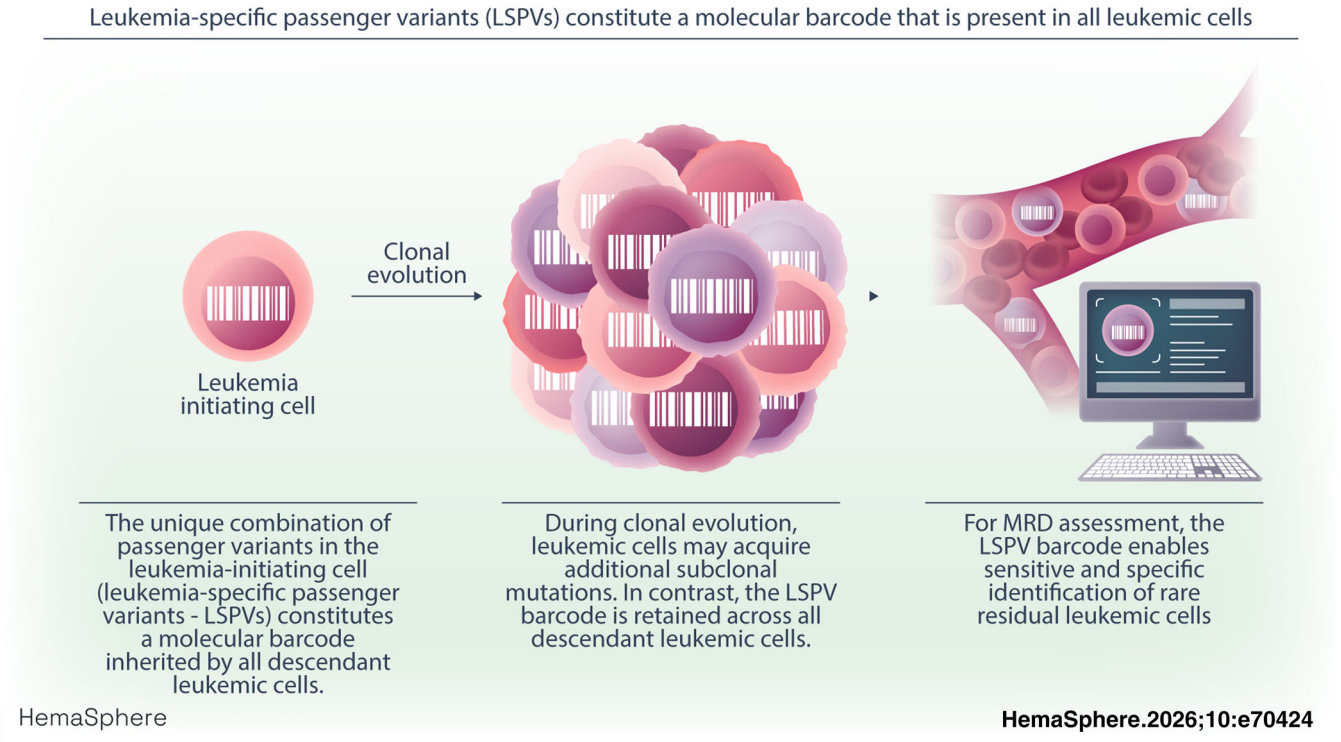

Received: 30 December 2025 | Accepted: 31 May 2026

DOI: 10.1002/hem3.70424

ARTICLE

HemaSphere eha

Passenger variants as pan-clonal markers of pediatric AML: Implications for molecular MRD

Ruth Shiloh[1,2,^] | Dana Dayan[3,4,^,] | Ifat Geron[1,2] | Maor Cohen[2,5] | Tamar Feuerstein[1] | Jorge Cano-Nistal[3,4] | Nurit Gal-Mark[1,2] | Shlomit Barzilai-Birenboim[1,6] | Dafna Gaash[1] | Michal Hameiri-Grossman[1] | Avraham Kahan[3,4] | Jamal Mahajna[5] | Nino Oniashvili[1] | Hava Rosenfeld[1] | Dan Scharf[3,4] | Keren Shichrur[1] | Elena Shinderman-Maman[1] | Sarah Elitzur[1,6] | Yehudit Birger[1,2,6] | Shai Izraeli[1,2,6,^] | Yosef E. Maruvka[3,4,^]

Correspondence: Shai Izraeli (sizraeli@gmail.com) and Yosef E. Maruvka (yosi.maruvka@bfe.technion.ac.il)

Abstract

A streamlined, sensitive, and universal molecular method for MRD detection in pediatric AML remains an unmet clinical need. Here, we propose a novel approach based on tracking somatic non-coding passenger variants. Using whole-genome sequencing (WGS) of diagnostic bone marrow DNA, we identify patient-specific somatic passenger variants, which we term "leukemia-specific passenger variants" (LSPVs). Single-cell DNA proteogenomic analyses demonstrate that LSPVs are specific and robust markers of leukemic cells, present across the entire leukemic cell population. Moreover, we show that LSPVs are accurate markers of disease burden, stable from diagnosis to relapse. Importantly, LSPVs can be detected in all patients, suggesting the universal applicability of this approach. Leveraging these findings, we developed DAISY-MRD, a streamlined WGS-based MRD method that does not rely on the presence of specific trackable genetic aberrations and does not require tailored assay design, making it simple, efficient, and feasible in clinical settings.

INTRODUCTION

In pediatric acute myeloid leukemia (AML), measurable residual disease (MRD) is the most powerful prognostic indicator for relapse and overall survival, and therefore serves as the basis for risk-adapted therapy.[1,2] However, the substantial biological and genetic heterogeneity of pediatric AML[3,4] presents challenges to the standardization of MRD assessment.

The current standard for MRD assessment in pediatric AML is multiparameter flow cytometry (MFC), which identifies leukemic blasts based on aberrant surface marker expression.[5,6] However, the specificity of MFC-MRD is limited by the similarity between AML blasts and normal myeloid progenitors, by the fact that not all leukemic cells express the same markers, and by treatment-related immunophenotypic shifts. Thus, even though MFC-MRD negativity after induction therapy is associated with improved prognosis, a considerable proportion of these patients relapse, underscoring the limited negative predictive value of this approach.

An alternative MRD approach uses quantitative RNA-based polymerase chain reaction (RT-qPCR) to track leukemia-specific genetic aberrations such as *PML*::*RARA*, *RUNX1*::*RUNX1T1*, *CBFB*::*MYH11*, and *NPM1* mutations.[7,8] Although highly sensitive and specific, this method is applicable only to a subset of patients carrying these aberrations. At the DNA level, recurrent pathogenic mutations can be identified at

[1]The Rina Zaizov Division of Pediatric Hematology-Oncology, Schneider Children's Medical Center, Petah Tikva, Israel
[2]Felsenstein Medical Research Center, Tel Aviv University, Rabin Medical Center, Petah Tikva, Israel
[3]Department of Biotechnology and Food Engineering, Technion, Haifa, Israel
[4]Lokey Center for Life Science and Engineering, Technion, Haifa, Israel
[5]Department of Biotechnology, Faculty of Sciences, Tel-Hai University of Kiryat Shmona in the Galilee, Kiryat Shmona, Israel
[6]Gray Faculty of Medical and Health Sciences, Tel Aviv University, Tel Aviv, Israel
Present addresses: Dana Dayan, Yale University, New Haven, Connecticut, USA; Ifat Geron, Sheba Medical Center, Ramat Gan, Tel Hashomer, Israel; Sarah Elitzur, St. Jude Children's Research Hospital, Memphis, Tennessee, USA.
[^]These authors contributed equally to this work.

diagnosis and monitored by targeted sequencing.[9] However, pathogenic mutations frequently reflect leukemic sub-clones that may disappear over the course of treatment and do not necessarily indicate the true risk of relapse.[10,11] This highlights the need for pan-clonal molecular markers for MRD assessment, defined here as markers present across the entire leukemic population. Such markers capture all leukemic cells and provide a more stable and reliable indicator of disease persistence. DNA-based monitoring of leukemia-initiating chromosomal breakpoints can achieve this,[12] but is technically demanding, requires patient-specific assays, and is not applicable for all patients.

Pathogenic mutations that drive proliferation or confer a fitness advantage can appear and disappear as the leukemic population evolves, particularly under treatment pressure. In contrast, genomic markers that have no biological effect are not subject to positive or negative selection. Thus, they are more likely to persist stably across all leukemic cells, effectively tagging the entire malignant population. This rationale is exemplified in acute lymphoblastic leukemia (ALL), where MRD is commonly assessed by quantifying leukemia-specific clonal V(D)J rearrangements, which are independent of the leukemia-driving mutations, but serve as a stable marker of the full leukemic clone.[13] Currently, no equivalent universal genetic marker is available for MRD monitoring in AML.

Mutations in DNA can normally be acquired in each cell division. While most mutations have no biological effect ("passenger variants"), they can serve as a marker for a specific cell and its progeny. As leukemia arises from a single cell, all passenger variants present in this cell at the time of transformation will be passed on to its progeny and may serve as a "molecular barcode" shared by all leukemic cells. In this study, we use whole-genome sequencing (WGS) of diagnostic bone marrow DNA to identify a set of high-confidence, pan-clonal somatic passenger variants unique to each patient's leukemia, which we term "leukemia-specific passenger variants" (LSPVs). We demonstrate that LSPVs serve as specific and prognostically relevant MRD markers that can be followed at high sensitivity using targeted sequencing. Moreover, using LSPVs, we present a streamlined method for MRD assessment using WGS. This approach does not rely on the presence of specific trackable genetic aberrations and does not require tailored assay design, making it simple, efficient, and universally applicable for all patients.

RESULTS

Genomic overview

WGS was performed at an average coverage depth of ×100 on DNA extracted from diagnostic bone marrow samples and matched T-cell DNA from each patient. T-cell DNA was used as a germline control to exclude germline variants. The tumor mutational burden (TMB) was low, with a median of 0.313 mutations/Mb, in agreement with previous reports[14] (Figure 1A). A positive correlation between age and TMB at diagnosis was observed ($r = 0.447$, $P = 0.022$, Supporting Information S1: Figure 1A). The frequency of pathogenic coding mutations was also low, in line with previous reports.[3] To assess driver gene influence, we compiled a list of 165 recurrently mutated driver genes in pediatric and adult AML using the COSMIC database and other published studies[3,11,14–18] (Supporting Information S12: Table 1). Of these, 28 were found to be mutated in our cohort, with *WT1* mutated in the largest number of patients ($n = 4$), followed by *FLT3* ($n = 3$). Most patients ($n = 20$) harbored between 0 and 3 driver gene mutations (Figure 1A and Supporting Information S1: Figure 1B).

We performed a mutational signature analysis using SigProfiler. Five signatures were identified, with a similar pattern displayed across patients (Figure 1A). SBS5, associated with aging, was present in every sample and accounted for the largest share of mutations on average (63.6%). No association was found between mutational signature at diagnosis and the risk of relapse.

Identification of patient-specific LSPVs

We defined LSPVs as passenger variants that are present in all leukemic cells at the time of diagnosis (pan-clonal variants). To distinguish pan-clonal from sub-clonal variants, we fitted the variant allele frequencies (VAFs) of all somatic variants using a Gaussian mixture model (GMM) to identify the combination of Gaussian curves that best described the data (see Methods). The curve whose mean was proportional to the patient's blast percentage was assumed to represent pan-clonal variants (Figure 1B and Supporting Information S2: Figure 2). To focus on passenger variants, coding mutations were excluded.

The number of identified LSPVs varied between patients, from a minimum of 60 to a maximum of 1777 (median ≈ 300), in line with the high inter-patient heterogeneity of pediatric AML (Figure 1C). LSPVs were evenly distributed across the genome (Supporting Information S3: Figure 3A). Similar to TMB, a positive correlation between age and the number of LSPVs was observed ($r = 0.460$, $P = 0.018$. Supporting Information S3: Figure 3B).

To evaluate the stability of LSPVs throughout disease progression, we performed WGS on DNA from relapse bone marrow samples of patients who experienced relapse. In the majority of relapsed patients (16/19), a substantial amount of LSPVs persisted at relapse, with an average of 79% and a median of 87% (Figure 1D). Out of the 3 patients for whom there was very little (<15%) persistence of LSPVs at relapse (Figure 1D, marked by an asterisk symbol), 2 patients (patients 284 and 291) experienced an isolated CNS relapse, accounting for the lack of disease burden in the bone marrow. The third patient (patient 239) experienced a bone marrow relapse after an extremely long remission period (62 months). Further genomic analysis of this patient's diagnostic and relapse samples identified a single shared ancestral CEBPA p.Lys313dup mutation, with otherwise mutually exclusive variant profiles. This pattern is consistent with independent evolution from a persistent pre-leukemic clone rather than relapse of the original leukemia. Overall, the high rate of persistence between diagnosis and relapse affirms that LSPVs are stable markers of the leukemic clone, suitable for disease monitoring.

LSPVs are specific markers of the entire leukemic cell population

Next, we sought to further characterize the variants classified as LSPVs to evaluate their potential as reliable pan-clonal markers. To explore their patterns of occurrence, we applied single-cell DNA proteogenomics (scDNA proteogenomics), a method that enables correlation of genotype with immunophenotype at the single-cell level.[17,19]

scDNA proteogenomics was performed on a diagnostic bone marrow sample from patient 297, using a custom panel tailored to follow patient-specific LSPVs and oligo-conjugated antibodies targeting relevant cell-surface markers. Cells were clustered based on the genotypes of 20 patient-specific LSPVs, and two clear clusters emerged, corresponding to cells that were either entirely wild type or uniformly mutated across all variants (Figure 2A, DNA panel). These results indicate that LSPVs co-occur together in the same single cells, and that LSPVs define a specific cell population. The proportion of the

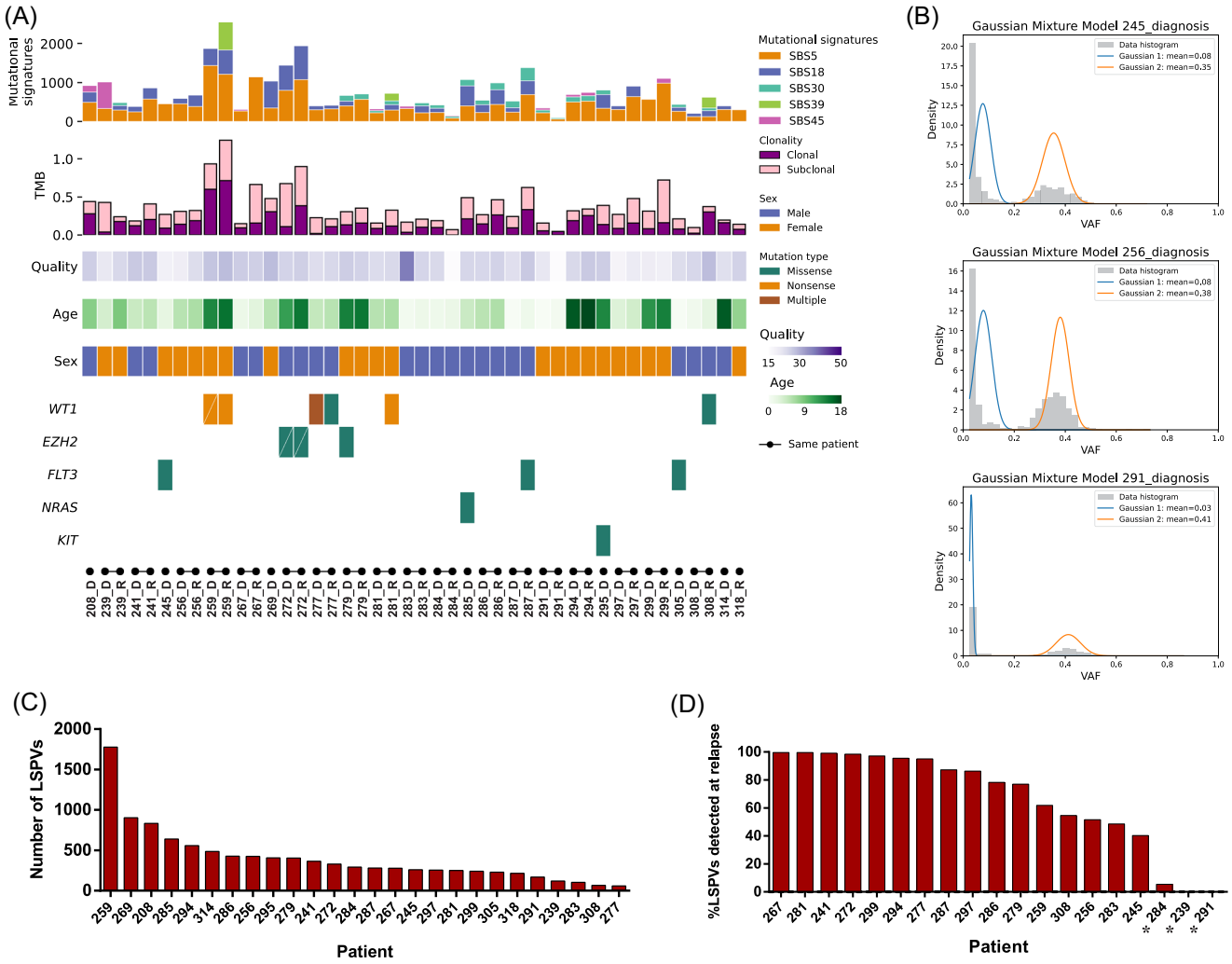

FIGURE 1 **Genomic overview and LSPV characteristics. (A)** CoMut plot describing the main characteristics of WGS samples. Samples organized by patient study ID number. Each column corresponds to an individual sample, with paired diagnosis and relapse samples aligned sequentially (D, diagnosis sample; R, relapse sample). Panels (top to bottom): Sig-profiler de novo extraction of mutational signatures; tumor mutational burden (TMB), colors represent the proportion of clonal and subclonal mutations; quality of Ultima Genomics WGS; patient age; patient sex; and recurrently altered genes, colored tiles indicate mutation type (missense, nonsense, or multiple). **(B)** Gaussian mixture model (GMM) plots showing the variant allele frequency (VAF) distributions of all somatic variants in three representative patients. The curves with the higher mean (orange) represent pan-clonal variants. GMM plots of all other patients are shown in Supporting Information S2: Figure 2. **(C)** Bar plot showing the number of LSPVs identified per patient. **(D)** Bar plot showing the percentage of patient-specific LSPVs identified by WGS in relapse bone marrow samples. Patients with <15% persistence of LSPVs at relapse are marked with an asterisk. LSPV, leukemia-specific passenger variants; WGS, whole-genome sequencing.

LSPV-mutated cluster was similar to the percentage of leukemic cells, as estimated by flow cytometry (Figure 2A, DNA panel and Supporting Information S4: Figure 4A), suggesting that the LSPV-mutated population corresponds to the leukemic cell population. Indeed, LSPV-mutated cells showed clearly distinct immunophenotypic patterns compared to LSPV-WT cells (Figure 2A, Protein panel). Specifically, LSPV-mutated cells showed dim expression of CD45 compared to LSPV-WT cells, consistent with the typical immunophenotype of leukemic blasts. In addition, LSPV-mutated cells were positive for CD34, CD117, and HLA-DR, and partially positive for CD56, similar to the leukemia-associated immunophenotype that was identified by flow cytometry for this patient (Figure 2A, Protein panel and Supporting Information S4: Figure 4B). In contrast, the LSPV-WT population showed high expression of CD45, was negative for CD34, CD117, and HLA-DR, and positive for mature lymphocytic markers such as CD3 and CD19, suggesting that these are nonleukemic lymphoid cells (Figure 2A, Protein panel). Overall, these results suggest that LSPVs are predominantly associated with leukemic cells.

To assess the extent to which LSPVs are shared across the leukemic cell population, we used cell-surface protein expression data to cluster the cells based on their immunophenotypes. This analysis revealed a clear leukemic cluster, as well as clusters of normal B- and T-cells (Figure 2B,C). Overlay of the genotype data on this UMAP revealed that the leukemic cluster was predominantly LSPV-mutated, whereas the B- and T-cell clusters were not (Figure 2D). Overall, these results indicate that LSPVs are specific to leukemic cells and are present across the entire leukemic cell population. Moreover, they suggest that different LSPVs serve as redundant markers for the leukemic clone, as they co-occur together in the same cells.

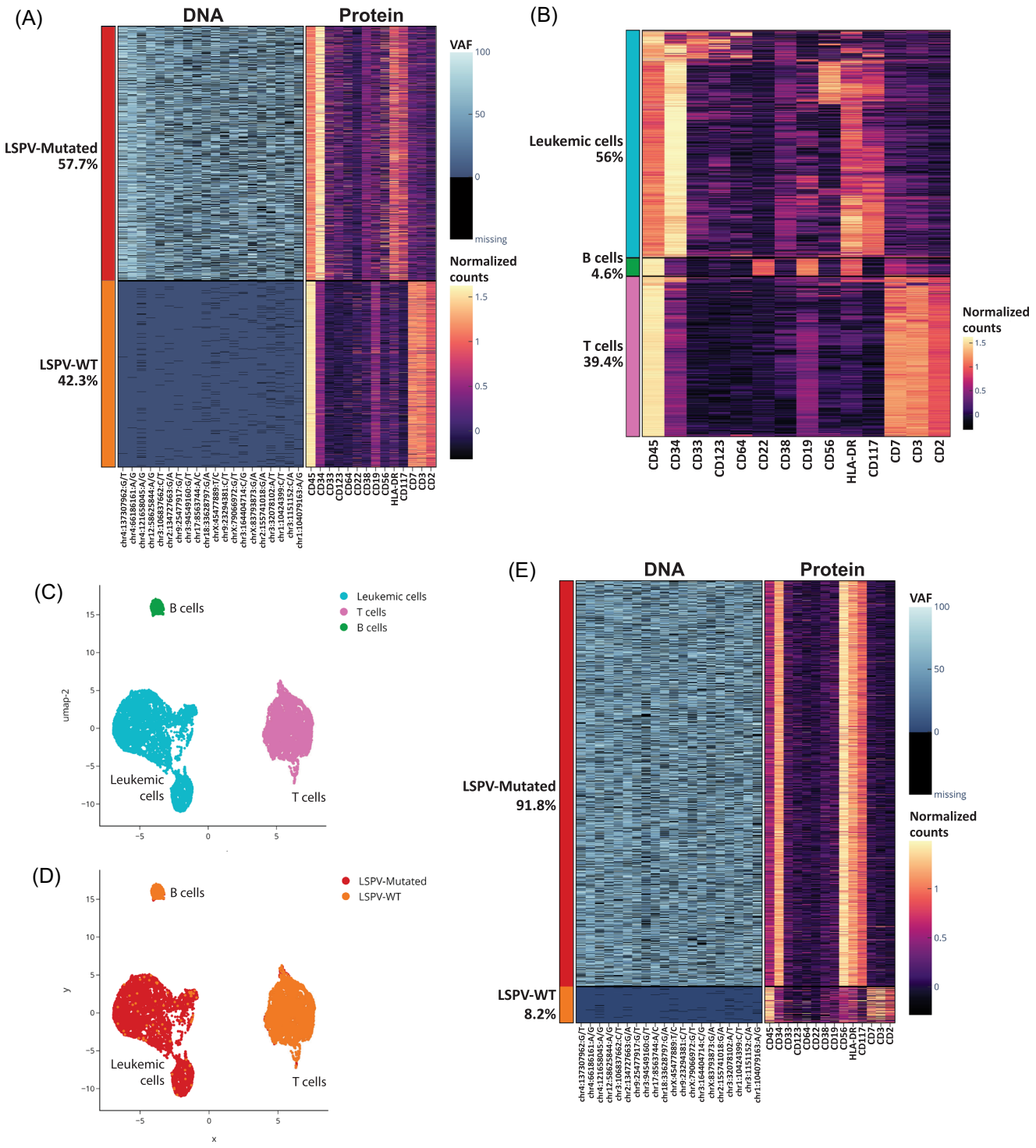

FIGURE 2 **Characterization of LSPVs at the single-cell level. (A)** Heat map showing combined genotype and immunophenotype data from the diagnostic bone marrow sample of patient 297. Each row represents a single cell (n = 15,832). DNA panel (left): each column represents an LSPV locus (n = 20). Colors represent whether each locus is wild type (dark blue) or mutated (light blue). Black marks loci where genotype calls were filtered out due to insufficient coverage or quality. Protein panel (right): each column represents a cell-surface marker (n = 14). Colors represent cell-surface expression intensity, with yellow indicating high expression and dark purple indicating low expression. Cells were clustered based on genotypes of 20 LSPVs and cell clusters were annotated as "LSPV-WT" or "LSPV-mutated." **(B)** Heat map showing immunophenotype data from the diagnostic bone marrow sample of patient 297, with cells clustered by immunophenotype. Each row represents a single cell (n = 15,832) and each column represents a cell-surface marker (n = 14). Colors represent cell-surface expression intensity, with yellow indicating high expression and dark purple indicating low expression. Cells were clustered based on cell-surface protein expression data and cell clusters were annotated based on known cell-surface markers of each cell population. (**C**) UMAP visualization of the cell clusters from **(B)**. **(D)** Overlay of DNA clone labels on the UMAP from **(C)**. Red: LSPV-mutated cells; Orange: LSPV-WT cells. **(E)**. Heat map showing combined genotype and immunophenotype data from the relapse bone marrow sample of patient 297, with cells clustered by genotype. Data shown in the same format as in **(A)**. (n = 12,688 cells).

Next, we utilized scDNA proteogenomics to evaluate whether the genotype–immunophenotype link remains robust despite immunophenotypic shifts that may occur between diagnosis and relapse. Flow cytometry analysis demonstrated that this patient showed an immunophenotypic shift at relapse: while at diagnosis only a subset of the leukemic cells was positive for CD56, at relapse, all leukemic cells were strongly positive for CD56 (Supporting Information S4: Figure 4A–D). Again, the same set of 20 LSPVs was uniformly mutated in a subset of cells, similar in size to the percentage of leukemic cells, as estimated by flow cytometry (Figure 2E, DNA panel and Supporting Information S4: Figure 4C). Importantly, the immunophenotypic shift was clearly observed in the single-cell data, where the LSPV-mutated cluster, which was only partially positive for CD56 at diagnosis (Figure 2A), displayed uniformly strong positivity for CD56 (Figure 2E, protein panel). These data demonstrate that LSPVs remained robust markers of the leukemic population at relapse, despite the immunophenotypic shift.

LSPVs are accurate markers of disease burden

Next, we aimed to investigate whether LSPVs can be used to quantify disease burden. As the VAF of the leukemia-initiating event is considered the most reliable molecular marker for disease burden, we selected 5 patients who carried different recurrent structural rearrangements, considered as leukemia-initiating aberrations. We hypothesized that if LSPVs are indeed specific markers of the entire leukemic cell population, their VAF at any time point should be identical to that of the leukemia-initiating event. To test this hypothesis, we inferred the genomic breakpoint sequence of the structural rearrangement from the WGS data and validated it by PCR. Next, we designed specific droplet digital PCR (ddPCR) assays for the structural rearrangements, as well as for 2–3 LSPVs per patient. Multiple time points were analyzed per patient, including diagnosis, relapse (if occurred), and remission. Notably, for every patient, different LSPVs showed near-identical VAFs at all measured time points, suggesting again that LSPVs serve as redundant markers of the same cell population (Supporting Information S5: Figure 5). Remarkably, the average VAF of the selected LSPVs was also near-identical to that of the initiating event, suggesting that these variants can serve as markers for disease burden (Figure 3A–E). Of note, ddPCR was employed to provide a unified quantitative platform for both structural rearrangements and point mutations. The achievable sensitivity for recurrent fusions may therefore be lower than that of optimized clinical RT-qPCR assays. Accordingly, comparisons between LSPVs and established molecular MRD markers should be interpreted primarily in terms of concordance in disease kinetics rather than absolute detection limits. Interestingly, there was one exception in which there was a discordance between the average LSPV VAF and that of the initiating event. For one of the patients, the measured VAF of the t(8;21) translocation at relapse was 67% (Figure 3D). As molecular estimation of blast percentage assumes a heterozygous state, a VAF exceeding 50% precludes reliable estimation. Conversely, the average LSPV VAF measured at this time point was 43%, consistent with 86% leukemic cells. Flow cytometry analysis of the relapse sample indicated a similar level of 84% leukemic cells, supporting the calculated LSPV VAF (Supporting Information S6: Figure 6). SNP array analysis revealed a sub-clonal deletion on chromosome 10 encompassing the RPP30 locus used as the diploid reference in ddPCR assays, resulting in overestimation of the fusion VAF (Supporting Information S7: Figure 7). This example highlights the potential caveats of using a single molecular marker to measure disease burden, as copy number alterations in a specific genetic locus may lead to errors. In contrast, using multiple redundant molecular markers that are distributed across the genome, such as LSPVs, helps avoid errors caused by copy number alterations at a single locus.

To compare the accuracy of LSPVs as markers of disease burden with that of pathogenic driver mutations, we selected a patient in whom a KIT D816Y mutation was identified at diagnosis at a high VAF using routine diagnostics. Using ddPCR, we measured the VAF of the KIT D816Y mutation as well as three different LSPVs at diagnosis, relapse, and multiple remission time points. This analysis revealed that the LSPV VAF was slightly higher than that of the KIT D816Y mutation at diagnosis (42% vs. 37%) and at the MRD time point at day 31 (0.1% vs.

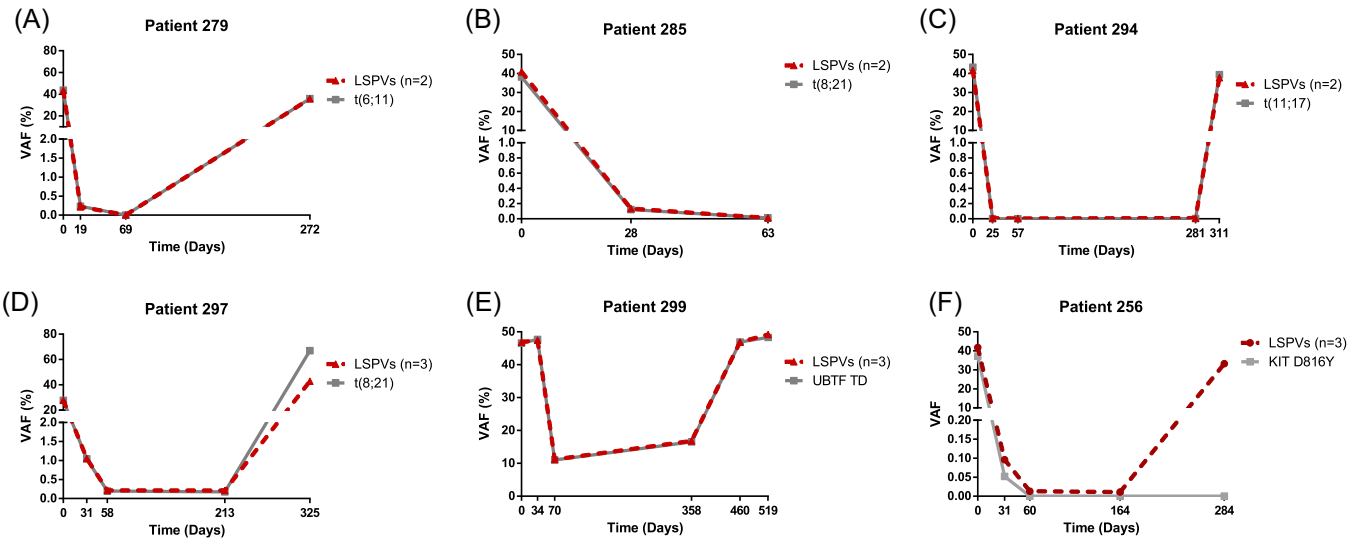

FIGURE 3 **LSPV frequency reflects leukemic disease burden. (A–E)** Graphs depicting the VAF of the leukemia-initiating chromosomal rearrangement (gray) and the mean VAF of 2-3 patient-specific LSPVs (red), as measured by ddPCR over time. **(F)** Graph depicting the VAF of the KIT D816Y mutation (gray) and the mean VAF of 3 patient-specific LSPVs (red), as measured by ddPCR over time. ddPCR, droplet digital polymerase chain reaction; LSPV, leukemia-specific passenger variants; VAF, variant allele frequencies.

0.05%) (Figure 3F). Remarkably, while the LSPVs re-emerged at a high VAF at relapse (33%), the KIT D816Y mutation was undetected. These results underscore the limitations of using driver mutations for disease monitoring in pediatric AML, as these mutations are often sub-clonal and may be lost during clonal evolution, even when present at high VAF at diagnosis. In contrast, LSPVs remain stable throughout disease evolution and re-appear at relapse, making them superior markers of disease burden and potential MRD targets.

LSPVs have prognostic value and enable WGS-based MRD surveillance

Next, we aimed to test whether LSPVs have prognostic value. To this end, we measured the VAF of 2-3 LSPVs per patient by ddPCR approximately 30 days after the initiation of induction chemotherapy. Again, different LSPVs of each patient showed near-identical VAFs, reconfirming the conclusion that LSPVs serve as redundant markers for the leukemic cell population (Supporting Information S8: Figure 8). Importantly, LSPV-MRD values were significantly higher in relapsed patients, suggesting that LSPV frequency is associated with the risk of relapse (Figure 4A).

Although targeted sequencing enables highly sensitive and specific mutation monitoring, its application in clinical settings is limited by the need to develop custom assays for each patient. In this respect, nontargeted sequencing approaches such as WGS are advantageous. However, the main limitation of WGS for MRD assessment is its limited sequencing depth, which may be insufficient to confidently detect variants present at very low allele frequencies (<1%). Therefore, WGS is not suitable for MRD monitoring that relies on the detection of one or a few specific molecular markers, as followed in most molecular MRD assays. In contrast, our results indicate that every patient harbors on average ~300 LSPVs, and that different LSPVs are redundant markers for the leukemic cell population. Therefore, all LSPV reads can be considered as independent measures of the same cell population and can be aggregated and measured together as one marker. To this end, we developed a WGS-based method for MRD surveillance: Distributed Analysis of Integrated Sites for Yielding MRD (DAISY-MRD). DAISY-MRD is a tumor-informed MRD detection approach that identifies LSPVs in diagnostic samples and monitors their presence in clinical remission samples. DAISY-MRD uses a WGS depth of approximately ×100. To remove noise, a multi-layered filtering strategy is applied to the LSPVs detected in the remission sample (see Methods). Then, reads across all LSPV positions are aggregated and the collective LSPV VAF (DAISY-MRD score) is calculated (Figure 4B). With an average coverage of ×100 and 300 LSPVs, this results in approximately 30,000 total reads, reaching a sensitivity applicable for MRD assessment. To estimate the background noise signal in DAISY-MRD, each patient's remission sample was compared against all other patients' LSPVs lists (see Methods). The 95th percentile of the noise distribution was defined as the upper limit of the expected background signal. This analysis resulted in a limit of detection of 3.3×10^{-4}.

The DAISY-MRD pipeline was applied to remission samples from approximately 30 days after the initiation of induction chemotherapy. To evaluate the accuracy of the DAISY-MRD score, we compared it with ddPCR measurements. DAISY-MRD scores were highly correlated with ddPCR results ($r = 0.99$, $P = 8.45e^{-13}$, Figure 4C), indicating that the DAISY-MRD pipeline is reliable.

Next, we compared the DAISY-MRD score of relapsed patients ($n = 19$) and nonrelapsed patients ($n = 7$) in our cohort. Interestingly, patients who later suffered from a CNS relapse showed considerably lower DAISY-MRD values than patients who experienced bone marrow relapse, implying that the level of residual disease in the bone marrow at this time point may have limited negative predictive value for CNS relapse. Overall, relapsed patients showed significantly higher DAISY-MRD scores compared with nonrelapsed patients, and this difference was more pronounced after excluding CNS relapses (Figure 4D and Supporting Information S9: Figure 9A). An ROC analysis for relapse prediction based on DAISY-MRD scores yielded an AUC of 0.90, indicating excellent discriminatory power (Figure 4E).

To investigate the prognostic applicability of DAISY-MRD, patients were stratified into MRD-positive and MRD-negative groups by DAISY-MRD levels of 5×10^{-4}. DAISY-MRD-positive patients showed decreased event-free survival (EFS), which became statistically significant upon excluding CNS relapses (Figure 4F and Supporting Information S9: Figure 9B). While overall survival was also lower in the DAISY-MRD-positive group, the difference was not statistically significant (Supporting Information S9: Figure 9C), probably due to the high percentage of relapsed patients who survived in this cohort following bone marrow transplantation (8/18, 44%) and the small patient number. While future studies using larger patient cohorts are necessary, altogether, these results indicate that DAISY-MRD has prognostic value and could potentially be used for MRD determination.

Discordance between genotype- and immunophenotype-based MRD assessment underscores differences between MFC-MRD and molecular approaches

To retrospectively compare DAISY-MRD with the current gold standard of MFC-MRD, we performed flow cytometry analyses at diagnosis and at MRD time points for 6 patients (3 relapsed and 3 nonrelapsed) for whom sufficient material was available (samples were collected between 2000 and 2014, when MFC-MRD was not part of routine diagnostics). In 4 out of the 6 cases, there was concordance between DAISY-MRD and MFC-MRD, with both methods classifying the patients who later relapsed as MRD-positive and the patients who did not relapse as MRD-negative (Figure 5A). However, 1 patient who subsequently relapsed was identified as MRD-positive only by DAISY, while no blasts were detected by flow cytometry. Additionally, in 1 patient who did not relapse, flow cytometry analysis was considered inconclusive due to a large population of immature cells and an abnormal differentiation pattern not fully matching the leukemic immunophenotype observed at diagnosis. Consequently, MFC-MRD could not be determined, whereas DAISY-MRD was negative. These observations suggest that tracking genetically defined leukemic clones by DAISY may offer greater specificity for residual leukemic cells than MFC-MRD.

To further investigate the relationship between the LSPV-mutated genotype and immunophenotype at an early postinduction MRD time point, we performed single-cell proteogenomic profiling of an MRD-positive bone marrow sample obtained from patient 297 on Day 31 post-induction and compared the results with MFC-MRD. This analysis revealed a complex and partially discordant relationship between genotype- and immunophenotype-based MRD assessment at this early posttreatment stage. Standard flow cytometry identified 0.2% residual blasts expressing high levels of CD34 (Figure 5B). In contrast, single-cell analysis identified 2.3% of the cells as LSPV-mutated (Figure 5C, DNA panel), a proportion more consistent with the patient's DAISY-MRD score (1.6% of cells, Figure 5A) than with the flow cytometry estimate.

The basis for this discordance becomes apparent upon examination of protein expression, as the LSPV-mutated cluster does

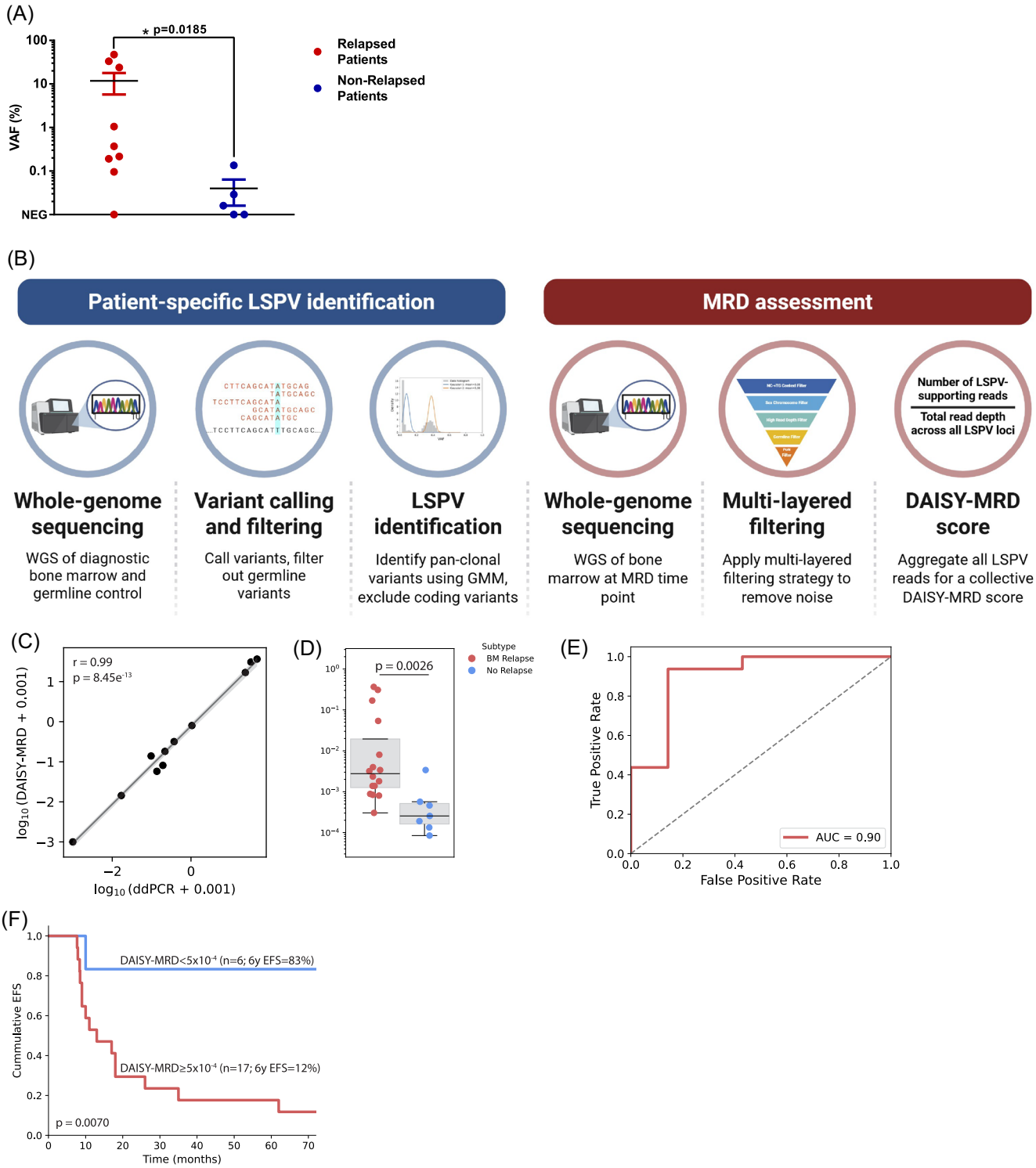

FIGURE 4 **DAISY-MRD shows potential prognostic value for relapse prediction.** **(A)** Dot plot depicting the mean LSPV VAFs measured by ddPCR at approximately Day 30 after the initiation of induction chemotherapy (relapsed patients: $n = 9$, nonrelapsed patients: $n = 5$). Statistical significance was calculated using the Mann–Whitney test. **(B)** Illustration of the DAISY-MRD pipeline. **(C)** Correlation between MRD values calculated by DAISY-MRD and by ddPCR. Correlation and statistical significance calculated using the Pearson correlation test. **(D)** Boxplot showing the $\log_{10}$-transformed DAISY-MRD values at approximately Day 30 after the initiation of induction chemotherapy of relapsed and non-relapsed patients (excluding isolated CNS relapses), colored by clinical outcome. Red: BM relapse, blue: no relapse. The horizontal line within each box represents the median, the box boundaries indicate the interquartile range (IQR), and whiskers extend to 1.5× IQR. Statistical significance calculated using the Kruskal–Wallis test. **(E)** Receiver operating characteristic (ROC) curve demonstrating the ability of DAISY-MRD to distinguish between relapsed and non-relapsed patients (excluding isolated CNS relapses). **(F)** Cumulative event-free survival (excluding isolated CNS relapses) of patients stratified by a DAISY-MRD level of 5×10^{-4}. Statistical significance was calculated using the log-rank test.

(A)

Patient	Relapse status	DAISY-MRD (% cells)	MFC-MRD (% cells)
259	Relapsed	POS (0.68%)	NEG
286	Relapsed	POS (0.16%)	POS (0.41%)
297	Relapsed	POS (1.6%)	POS (0.2%)
269	Non-relapsed	NEG	Inconclusive (4.65%)
305	Non-relapsed	NEG	NEG
314	Non-relapsed	NEG	NEG

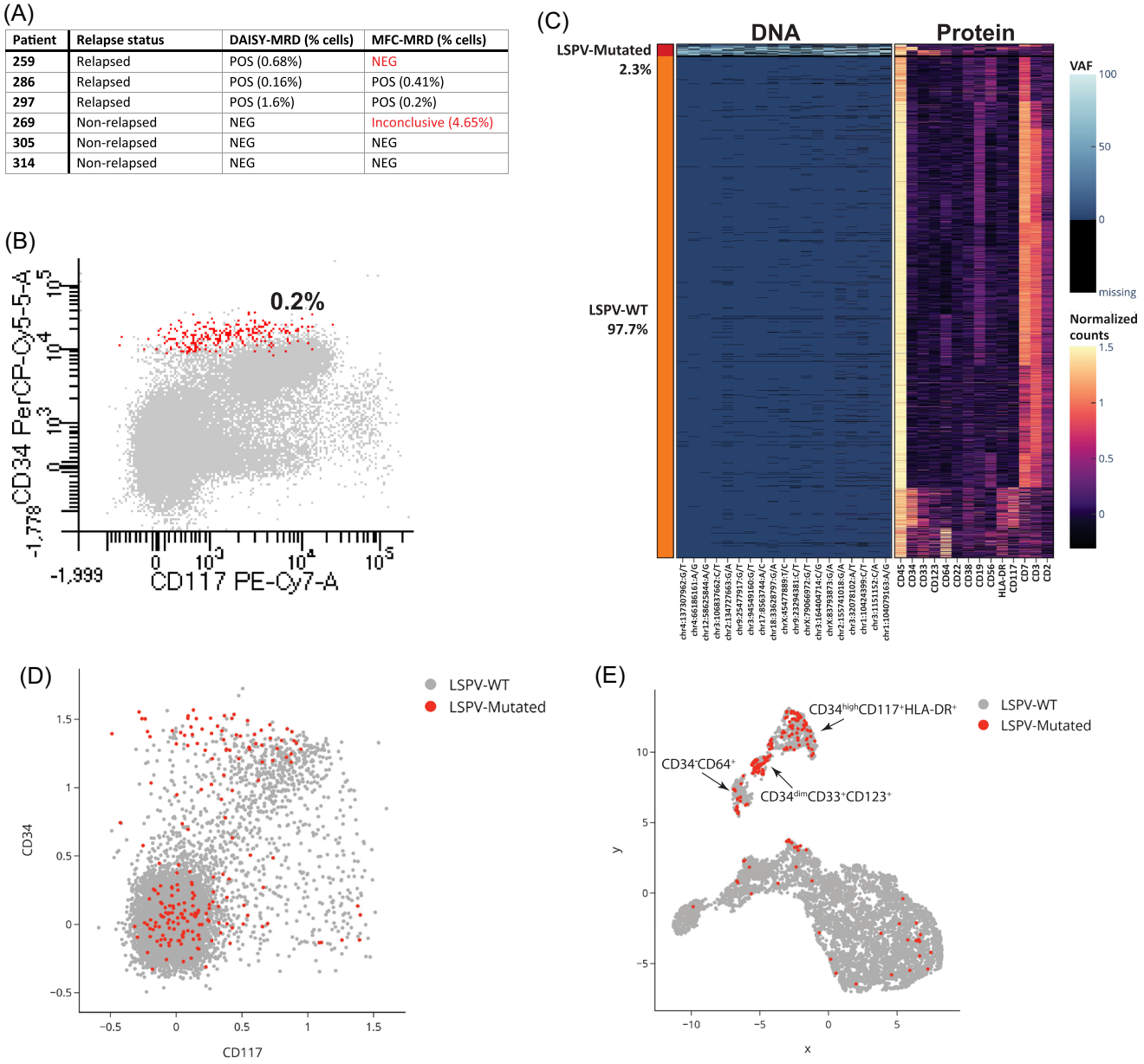

FIGURE 5 **Partial discordance between genotype and immunophenotype at the MRD time point**. **(A)** Table summarizing the comparison between DAISY-MRD and FACS-MRD results for 6 patients. To represent %cells, DAISY-MRD VAF was multiplied by 2. The cutoff below which DAISY-MRD was considered negative was 5×10^{-4} VAF. The cutoff below which FACS-MRD was considered negative was 0.1% cells. Discordant cases are marked in red. **(B)** Flow cytometry analysis of bone marrow mononuclear cells from patient 297 on Day 31 post-induction. Viable cells were gated according to the FS/SSC distribution. Leukemic blasts (red) were gated from viable cells according to high CD34 expression and their percentage was evaluated as 0.2%. **(C)** Heat map showing combined genotype and immunophenotype data from patient 297's Day 31 post-induction bone marrow sample, with cells clustered by genotype. Each row represents a single cell ($n = 8827$). DNA panel (left): each column represents an LSPV locus ($n = 19$). Colors represent whether each locus is wild type (dark blue) or mutated (light blue). Black marks loci where genotype calls were filtered out due to insufficient coverage or quality. Protein panel (right): each column represents a cell-surface marker ($n = 14$). Colors represent cell-surface expression intensity, with yellow indicating high expression and dark purple indicating low expression. Cells were clustered based on genotypes of 19 LSPVs and cell clusters were annotated as "LSPV-WT" or "LSPV-mutated." **(D)** A biaxial plot of CD34 and CD117 cell-surface expression was generated from single-cell proteogenomic data, with genotype data overlaid. **(E)** A UMAP was generated based on expression data of 20 cell-surface markers, with genotype data overlaid.

not show a homogeneous immunophenotype (Figure 5C, protein panel). Notably, there was only partial overlap between the LSPV-mutated clone and the $CD34^{high}$ population monitored by MFC-MRD (Figure 5D), with a substantial subset of LSPV-mutated cells lacking CD34 and CD117.

To further characterize the immunophenotypic landscape of the LSPV-mutated clone, cells were clustered based on immunophenotype and visualized using a UMAP with overlaid genotype data. This analysis revealed that the LSPV-mutated cells were predominantly distributed across three phenotypically distinct clusters: a $CD34^{high}CD117^{+}HLA\text{-}DR^{+}$ cluster (similar to the immunophenotype monitored by MFC-MRD), a $CD34^{dim}CD33^{+}CD123^{+}$ cluster, and a $CD34^{-}CD64^{+}$ cluster (Figure 5E and Supporting Information S10: Figure 10). Notably, although $CD34^{high}CD117^{+}HLA\text{-}DR^{+}$ was the predominant leukemic

immunophenotype at diagnosis, minor subpopulations with the additional immunophenotypes were already present at that time (Figure 2B). This suggests that these phenotypically distinct populations did not arise as a result of therapy, but may instead have been positively selected during treatment at this early post-induction time point. Continued selection during subsequent therapy is likely to further shape clonal phenotypic architecture, ultimately resulting in the expansion of the $CD56^+$ relapse clone observed at the later time point (Figure 2E). The observed discrepancy between MFC-MRD and molecular MRD underscores inherent methodological differences: MFC-MRD is biased toward detecting the main leukemia-associated immunophenotype and immature cells, whereas molecular approaches are not restricted to a specific immunophenotype. These results demonstrate that LSPV genotype-based MRD assessment captures phenotypically heterogeneous leukemic populations that may escape detection by MFC-MRD, thereby providing a more comprehensive measure of residual disease.

Collectively, our results suggest that LSPV genotype-based MRD enables specific identification of residual leukemic cells, while addressing limitations of existing immunophenotypic methods. Larger prospective cohorts will be required to systematically compare the two approaches and determine how DAISY-MRD performs across diverse patient samples and clinical contexts.

DISCUSSION

Developing a streamlined, sensitive, and universal molecular approach for MRD detection in pediatric AML remains an unmet clinical need. In this study, we developed an approach to robustly identify LSPVs, unique pan-clonal markers of pediatric AML that can be readily monitored for MRD using a simple workflow. Using single-cell DNA proteogenomics, we show that LSPVs serve as specific and redundant markers of leukemic cells, shared across the entire leukemic population. Using ultra-sensitive ddPCR, we demonstrate that LSPVs are highly accurate markers of disease burden, stable throughout disease progression from diagnosis to relapse. These properties make LSPVs highly suitable for MRD monitoring, and superior to current commonly used methods.

Current approaches for MRD assessment in AML, including flow cytometry and targeted sequencing, are limited in their ability to capture the entire leukemic cell population. Not all leukemic cells express the leukemia-associated immunophenotype used for MFC-MRD detection, and antigen expression may change during treatment, leading to immunophenotypic shifts.[20] Similarly, at the molecular level, pathogenic mutations identified at diagnosis are frequently sub-clonal, and clonal evolution during treatment can result in the disappearance of these variants at relapse.[10,11] Consequently, both flow cytometry and targeted sequencing may fail to detect certain leukemic cells, and negative MRD results may not reliably reflect the true risk of relapse. In contrast, our results demonstrate that LSPVs are highly stable and accurate markers of disease burden, present in the entire leukemic cell population, making them reliable MRD targets.

Our single-cell proteogenomics results suggest that while the correspondence between genotype and immunophenotype is highly concordant in overt disease, it becomes more heterogeneous in the post-treatment MRD setting, potentially reflecting therapy-driven selection within the residual leukemic compartment. These findings underscore the value of single-cell proteogenomics in resolving residual leukemic populations beyond conventional immunophenotypic definitions and highlight differences between immunophenotype- and genotype-based MRD approaches, as canonical gating strategies may fail to detect leukemic subsets lacking immature or predominant leukemia-associated immunophenotypes. The prognostic significance of residual mutated cells outside the immature $CD34^+$ compartment remains a matter of debate. Although AML leukemic stem cells (LSCs) were initially defined as $CD34^+CD38^-$,[21] subsequent studies have shown that LSC activity is not restricted to this compartment and can be detected across multiple immunophenotypic fractions, including $CD34^-$ populations.[22,23] As LSPVs effectively mark the entire leukemic cell population, they may be useful in future studies addressing these questions.

The concept of following a "molecular barcode" rather than leukemia-driving pathogenic variants resembles the approach successfully used in acute lymphoblastic leukemia (ALL), where MRD monitoring relies on following a specific V(D)J rearrangement as a stable marker of the leukemic clone.[13] This underscores the advantage of using non-pathogenic, clonally stable markers over potentially unstable driver mutations for more reliable MRD assessment.

Previous studies have used exome sequencing to identify patient-tailored, leukemia-specific mutations suitable for MRD monitoring.[24,25] While these studies established proof of concept for a personalized, DNA-based MRD approach in AML, the use of exome sequencing presented several limitations. Mutations detected by this method are frequently pathogenic coding variants, which are often sub-clonal and therefore less reliable as MRD markers. Moreover, only a limited number of leukemia-specific mutations can typically be identified per patient, necessitating ultra-deep targeted sequencing to achieve adequate sensitivity for MRD detection. In contrast, our WGS-based approach generally enables identification of hundreds of LSPVs per patient. The large quantity of such redundant MRD markers provides a unique opportunity to use WGS rather than deep targeted sequencing for MRD monitoring, thus considerably simplifying the workflow. WGS-based approaches such as DAISY-MRD are becoming increasingly feasible in clinical settings due to rapid reductions in sequencing costs and simplified, scalable workflows. Unlike ddPCR or flow cytometry, DAISY-MRD does not require specific assay design and optimization or operator-dependent interpretation, reducing labor and variability. Turnaround times are now compatible with clinical practice, and recent large real-world studies demonstrate that WGS can be implemented routinely and at scale in oncology diagnostics.[26] Further decreases in sequencing costs may enable WGS at ×1000, allowing detection of residual disease at levels approaching 10^{-5}.

Of particular importance, our data suggest that LSPVs can be detected in all patients, suggesting the universal applicability of this approach. Currently, a suitable method for MRD assessment is lacking for some patients, for example, cases in which leukemic cells do not show a distinguishable leukemia-associated immunophenotype or cases lacking trackable molecular markers. Utilizing LSPVs for MRD assessment offers a promising approach for these patients.

A key difference between pediatric and adult AML is the presence of a prolonged preleukemic phase in adult AML, associated with clonal hematopoiesis. It has been shown that preleukemic mutations may persist after successful treatment without clearly affecting relapse risk. Therefore, such mutations are generally excluded from MRD assessments.[9,27] A potential caveat in our approach is the possible misidentification of pre-leukemic variants as LSPVs, leading to their inclusion in MRD assessment and a consequent overestimation of the true MRD burden. As pediatric AML is not typically associated with a prolonged pre-leukemic phase and clonal hematopoiesis, this is unlikely. Indeed, in this study, LSPVs were not detected in non-relapsed patients, suggesting that they are not preleukemic, and DAISY-MRD scores, calculated based on all LSPVs, had excellent discriminatory power between relapsed and non-relapsed patients.

We hypothesize that in adult cases involving clonal hematopoiesis, any preleukemic variants inadvertently classified as LSPVs might persist or expand after treatment. Such behavior could give rise to a bimodal distribution of VAFs at MRD time points, with true LSPVs tending to show lower VAFs than pre-leukemic variants. Addressing this possibility may require a dedicated computational framework designed to distinguish these patterns. However, this question remains to be resolved in studies specifically focused on adult AML.

Some of the conclusions of this study are limited by the relatively small cohort of patients. Larger studies, conducted under contemporary treatment protocols and incorporating standardized MRD time points, will be necessary to further evaluate this approach for MRD monitoring and for determination of prognostically significant cut-offs. However, our data propose LSPVs as promising targets for MRD monitoring, allowing a specific and sensitive molecular MRD measurement that is universally applicable for all patients, while overcoming several limitations of existing methods.

METHODS

Patients

This study includes 26 pediatric patients (13 males and 13 females) who were diagnosed with AML at Schneider Children's Medical Center between 2000 and 2014 (median age at diagnosis 5.6 years, range 0.4–17.9 years). Children were treated according to the AML-BFM-98 protocol. 19 patients relapsed, while 7 patients remained in complete remission following treatment. Patients were selected based on the availability of cryopreserved samples. Patients who remained in complete remission following upfront allogeneic bone marrow transplantation were excluded. Cases of acute promyelocytic leukemia with t(15;17)(q22;q12); *PML::RARA* were also excluded. The study was conducted in accordance with the Declaration of Helsinki and was carried out according to local guidelines and regulations. Patient characteristics are summarized in Table 1.

T-cell isolation and expansion

T-cells were separated from bone marrow mononuclear cells using CD3 magnetic beads (Miltenyi Biotech, #130-050-101) according to the manufacturer's protocol and then expanded in vitro in 24-well plates precoated with anti-CD3 (#130-093-387; Miltenyi Biotech). Cells were grown in RPMI 1640 (#01-100-1A-04; Biological Industries) supplemented with 10% FBS (#10270106; Gibco, Thermo Fisher Scientific), 4 mM L-glutamine (#25030024; Thermo Fischer Scientific), and 5 µg/mL anti-CD28 (#130-093-375; Miltenyi Biotech).

DNA extraction

Genomic DNA was extracted from bone marrow PBMCs and isolated T-cells using the QiaAmp DNA mini kit from Qiagen (#51304) and eluted in molecular-grade water.

Whole-genome Sequencing (WGS)

WGS was performed on genomic DNA from a total of 96 samples, comprising 70 pediatric AML bone marrow samples (including diagnosis, remission, and relapse time points) and 26 matched T-cell samples.

A total of 250 ng of genomic DNA per sample was used to generate PCR-free libraries using the Ultima Genomics (UG) ppmSeq protocol. DNA shearing was performed with the NEBNext UltraShear kit (M7634), followed by library construction using 2.5 µL of the Ultima ppmSeq Adapter and the NEBNext Ultra II DNA PCR-free Library Prep Kit (E7410), according to the manufacturer's instructions. Libraries were sequenced on the UG100 platform, producing 170 bp single-end reads using a mostly natural sequencing-by-synthesis chemistry with non-terminating nucleotides. A 65 pM library input yielded an average of $>2.5 \times 10^9$ reads per sample, achieving ×>100 average coverage depth. Reads were aligned to the GRCh38 (hg38) reference genome, and downstream analysis included somatic variant calling and structural variant (SV) detection.

TABLE 1 Patient characteristics.

Characteristic		All patients (n = 26)	Relapsed patients (n = 19)	Nonrelapsed patients (n = 7)
Age at diagnosis (years) Median (range)		5.6 (0.4–17.9)	5 (0.4–17.9)	8.1 (0.6–17.8)
Sex n (%)	Male	13 (50%)	9 (47%)	4 (57%)
	Female	13 (50%)	10 (53%)	3 (43%)
TTR (months) Median (range)		-	10 (6.3–62)	-
Cytogenetics n (%)	t(8; 21)	7 (26.9%)	4 (21%)	3 (43%)
	Normal karyotype	5 (19.2%)	3 (16%)	2 (29%)
	MLL rearrangement	4 (15.4%)	4 (21%)	0 (0%)
	Complex karyotype	3 (11.5%)	2 (11%)	1 (14%)
	inv(16)	2 (7.7%)	1 (5%)	1 (14%)
	UBTF TD	1 (3.8%)	1 (5%)	0 (0%)
	+8	1 (3.8%)	1 (5%)	0 (0%)
	del(9q)	1 (3.8%)	1 (5%)	0 (0%)
	t(5; 12)	1 (3.8%)	1 (5%)	0 (0%)
	+21	1 (3.8%)	1 (5%)	0 (0%)

Abbreviation: TTR, time to relapse.

Mutational calling

UG-tailored DeepVariant

We used the resulting cram files for the calling of variants using a tailored Googles' DeepVariant version for UGs' data. The minimum detection threshold was set at 3% allele frequency (AF) for WGS. We then applied a few postanalysis filtering steps.

Germline (gnomAD) filtering

To identify population variants, gnomAD version 4.0.1 was used. All variants were cross-referenced with the database, and those with an AF greater than 10^{-3} in the general population were considered likely germline and excluded from further analysis.

Panel of Normals (PoN) construction and filtering

To reduce recurrent technical artifacts from somatic variant call sets, a PoN was constructed using WGS data from 219 unrelated healthy individuals sequenced on the UG platform at an average depth of ×16. To generate this filter, we first compiled a comprehensive list of variant positions observed across all PedAML samples. For each site, we quantified read support for each nucleotide (A, C, G, T) across all normal samples using the samtools mpileup (version 1.17).

Because nonreference nucleotides at these sites can represent either sequencing artifacts or true germline variation, we applied a one-tailed binomial test in each normal sample at every candidate position. At each locus, the two most frequent alleles were identified, and a test was performed under the null hypothesis that both alleles can be seen with equal probability ($P = 0.5$). Positions with $P > 0.05$ were classified as germline and excluded, whereas positions with $P \leq 0.05$ were considered noise and retained for artifact modeling. As expected, germline variants displayed VAFs centered around ~0.5, while technical artifacts showed highly skewed VAFs near zero. Many apparent germline sites with VAF = 0 were attributable to the low mean coverage (×~3.14 per sample) in the normal cohort (Supporting Information S11: Figure 11).

For quality control, we required that retained positions have a total read depth of at least 300 across all normals and were observed in at least 30 individuals. For each such site, we estimated the probability of observing each alternative allele from the aggregated counts across normal samples. At each variant position in patient samples, we performed a one-tailed binomial test under the null hypothesis that the observed alternative allele frequency could be explained by the background error rate defined by the PoN. Variants with $P \leq 0.05$ were retained as likely somatic, while those with higher P-values were excluded as noise. This approach provides locus-specific artifact suppression based on empirical evidence from healthy individuals.

Variant Effect Predictor (VEP) annotation

The files were annotated using VEP with the GRCh38 assembly.

SV calling

SVs were identified using the UltimagenHealthOmics SV pipeline. This specialized workflow was implemented to detect larger genomic alterations that could not be reliably captured by the somatic mutation calling pipeline, particularly indels exceeding 30 bases in length.

The pipeline integrates multiple SV callers and implements filtering strategies to reduce false positives while maintaining high detection rates for clinically relevant variants.

Signatures' inference

A mutational signature pattern was generated for each cancer sample (diagnosis/relapse) using a 96-bin classification. These catalogs were analyzed using SigProfilerExtractor to identify de novo mutational signatures and quantify their activities across individual samples. The extracted signatures were then compared to known COSMIC mutational signatures to assess their similarity and infer their potential etiology.

Driver genes

A list of recurrently mutated driver genes was extracted from the COSMIC database, filtered to those that were found to be driver on adult or pediatric AML, and integrated with a list curated from published data.[3,11,14–18]

Selection of pan-clonal variants

The determination of pan-clonal or subclonal variants was performed using a GMM on the VAF distribution for each sample. Subsequently, the Gaussian component with the highest median VAF was selected and designated as the expected VAF for pan-clonal mutations. This value represents the probability that a sequencing read supports the mutation when it is present in all leukemic cells.

Given that we expect that pan-clonal variants will have a high VAF, we began with the null hypothesis that each variant was pan-clonal and then tested whether this assumption could be rejected. Specifically, we performed a one-sided binomial test with the alternative hypothesis "less," using the median of the higher Gaussian component as the success probability, the total number of reads covering the variant as the number of trials, and the number of mutation-supporting reads as the number of successes. We then calculated the probability of observing that number of supporting reads or fewer under the clonal model. Variants with $P < 0.05$ were classified as sub-clonal, whereas variants with $P \geq 0.05$ were treated as pan-clonal.

As a summary, for each sample, we inferred whether each locus-specific putative variant is pan-clonal or sub-clonal from its VAF using a two-stage procedure: (i) sample-level modeling of the VAF distribution with a GMM and (ii) locus-level hypothesis testing with a one-sided binomial test.

The analysis is described mathematically as follows:

1. GMM for VAF:

   Let V_i be the VAF for mutation i in a given patient. We model the distribution of V using a GMM with K components:

$$\textbf{GMM for VAF}: \; p(V) = \sum_{k=1}^{K} \pi_k N\left(V \middle| \mu_k, \sigma_k^2\right) \tag{1}$$

   where π_k are the mixture weights and $N(V|\mu_k, \sigma_k^2)$ represents a normal distribution with mean μ_k and variance σ_k^2.

2. Determination of the probabilistic threshold p_0:

   Define $p_k = \mu_k$ as the median VAF for each Gaussian component (since the median of a normal distribution is its mean).

The maximum median among the Gaussian components is given by

Determination of the probabilistic threshold p_0:

$$p_0 = \underbrace{\max_k}(p_k) = \underbrace{\max_k}(\mu_k) \quad (2)$$

This value p_0 represents the probability of a read supporting a mutation in the sample.

3. One-sided Binomial test:

For each mutation, let n be the total number of reads covering the site and x be the number of reads supporting a mutation. The probability of observing x or fewer successes under the null hypothesis $H_0 : p = p_0$ follows a binomial cumulative distribution function (CDF):

P–value of one–sided Binomial test :

$$p\_value = P(X \le x | n, p_0) = \sum_{j=0}^{x} \binom{n}{j} p_0^j (1 - p_0)^{n-j} \quad (3)$$

where j is the summation index representing the number of successes (mutants reads) from 0 to x.

4. Classification of mutations

A mutation is classified as **pan-clonal** if:

P–value threshold for mutation classification : $P \ge 0.05$ (4)

Otherwise, it is classified as **sub-clonal**.

DAISY-MRD

DAISY-MRD aggregates all reads covering all the positions of patient-specific LSPVs, treating them as independent measurements of the same biological signal. The final MRD score was calculated as the ratio between the summed LSPV-supporting reads and the total read covering LSPV loci.

To enhance the accuracy of MRD detection, a cumulative filtering strategy was applied to the LSPV list:

1. **NC → TG Context Filter:** Variants in NC → TG sequence contexts were excluded due to their known association with sequencing artifacts in UG data.
2. **Sex Chromosome Filter:** Variants on chromosomes *X* and *Y* were removed to avoid sex-specific biases.
3. **High Read Depth Filter:** Positions with a total read depth exceeding 200 were excluded as likely mapping artifacts.
4. **Germline Filter:** A one-tailed binomial test ($P > 0.01$) was used to remove likely germline variants.
5. **PoN-Based Filter:** A final filter using the PoN retained only variants with a locus-specific $P < 0.05$, indicating a signal significantly above the technical noise floor.

The DAISY-MRD code is available at: https://github.com/danadayan/daisy-mrd.

Signal-to-Noise and Statistical Analysis

To estimate the background noise signal in DAISY-MRD, each patient's remission sample was compared against all other patients' LSPVs lists. The 95th percentile of the noise distribution was defined as the upper limit of the expected background signal. This analysis resulted in a limit of detection of 3.3×10^{-4}.

Droplet-digital PCR (ddPCR)

For ddPCR analysis of LSPVs, specific primers and probes were designed for 3–5 LSPVs per patient and optimized using diagnostic DNA from the corresponding patient together with a temperature-gradient ddPCR assay. Assays producing clear and specific signal separation were selected for downstream analysis of patient samples (typically 2–3 assays per patient). LSPVs selected for ddPCR analysis met the following criteria: (i) pan-clonal VAF at diagnosis and at relapse (if occurred) according to WGS; (ii) not located on sex chromosomes; (iii) not located on chromosomes known to be structurally rearranged in the patient sample according to patient files; (iv) for each patient, selected LSPVs were located on different chromosomes; and (v) exclusion of C > T substitutions followed by G, to minimize potential artifacts related to cytosine deamination and sequencing bias. Reactions were performed according to the manufacturer's instructions. Briefly, 50–250 ng of genomic DNA was combined with ddPCR Supermix for Probes (no dUTP) (#186-3024; Bio-Rad Laboratories) and variant-specific primers and probes (PrimeTime Mini qPCR Probe Assay; Integrated DNA Technologies), and partitioned into approximately 20,000 nanoliter-sized droplets using the QX200 Droplet Generator. PCR amplification was performed on a C1000 Touch Thermal Cycler (Bio-Rad Laboratories), and droplets were analyzed using the QX200 Droplet Reader (Bio-Rad Laboratories). VAFs were calculated using QX Manager software 2.2 Standard Edition (Bio-Rad Laboratories). RPP30 (#10031243; Bio-Rad Laboratories) was used as a wild-type control for quantifications of genomic rearrangements. The KIT D816Y (c.2446G>T) mutation detection assay was purchased from Bio-Rad (#10049550). All reactions were performed in triplicates, and only results with ≥10,000 accepted droplets were included in the analysis. All primers and probes are listed in Supporting Information S13: Table 2.

Single-cell proteogenomics

Viably frozen bone marrow mononuclear cells were thawed and washed in staining media (HBSS, 2% FBS). Dead cells were removed using the Dead Cell Removal kit (#130-090-101; Miltenyi Biotech). Live cells were quantified using trypan blue. A total of 10^6 cells were resuspended in cell staining buffer (#420201; BioLegend) and incubated with TruStain FcX and Tapestri blocking buffer for 15 min on ice. Cells were then incubated with TotalSeq™-D scMRD AML Antibody Cocktail v1 spiked with TotalSeq™-D0048 anti-human CD45 Antibody (#368553; Biolegend) and TotalSeq™-D0162 anti-human CD64 Antibody (#305051; Biolegend) for 30 min on ice. Cells were then washed three times with cell staining buffer (#420201; BioLegend). Single-cell libraries were prepared according to the Mission Bio Tapestri® Single-Cell DNA + Protein Sequencing v3 protocol (Mission Bio). Targeted PCR amplification was performed using a custom panel of 218 amplicons, designed to cover patient-specific SNVs of patient 297 as well as a similar number of control SNVs that were found in another patient (patient 245). Libraries were quantified by Qubit (Thermo Fischer Scientific), analyzed using TapeStation (Agilent Technologies, Santa Clara, CA, USA), and pooled for sequencing on an Illumina NovaSeq (Illumina, Inc.) according to Mission Bio guidelines.

FASTQ files from scDNA + protein samples were processed via the Mission Bio Tapestri v3 pipeline (version 3.6). After pipeline processing, data for each run were aggregated into H5 files, which were analyzed using Mission Bio Python Mosaic (version 3.7).

Cell staining and flow cytometry analysis

Cells were stained with the following antibodies for 15 min in the dark: CD56 FITC (#345811; Becton, Dickinson and Company); CD34 PerCP-Cy5.5 (#347222; Becton, Dickinson and Company); CD117 PC7 (#IM3698; Beckman Coulter); HLA-DR Pacific Blue (#A74781; Beckman Coulter); and CD45 Krome Orange (#B36294; Beckman Coulter). After incubation, red blood cell lysis was performed using BD FACS Lysing Solution (#349202; Becton, Dickinson and Company) for 10 min, followed by two washing steps with PBS containing 2% FBS. Data acquisition was carried out using a FACS CANTO II flow cytometer, and analysis was performed using Diva software (Becton, Dickinson and Company).

Single-nucleotide polymorphism (SNP) array

SNP array analysis was performed using Affymetrix CytoScan HD array (Affymetrix) according to the manufacturer's recommendations (Affymetrix manual protocol Affymetrix® Cytogenetics Copy Number Assay P/N 703038 Rev. 3). The raw data were processed using the Chromosome Analysis Suite (ChAS) 4.5.0.34.

ACKNOWLEDGMENTS

The authors thank the patients and their families for participating in this study, as well as the physicians, nurses, and clinical staff involved in their care.

AUTHOR CONTRIBUTIONS

Ruth Shiloh: Conceptualization; investigation; writing—original draft; methodology; validation; visualization; data curation; formal analysis. **Dana Dayan**: Data curation; formal analysis; software; methodology; validation; writing—review and editing; visualization. **Ifat Geron**: Investigation; writing—review and editing; conceptualization. **Maor Cohen**: Investigation. **Tamar Feuerstein**: Investigation. **Jorge Cano-Nistal**: Software. **Nurit Gal-Mark**: Investigation. **Shlomit Barzilai-Birenboim**: Resources. **Dafna Gaash**: Methodology. **Michal Hameiri-Grossman**: Visualization; investigation. **Avraham Kahan**: Software. **Jamal Mahajna**: Supervision. **Nino Oniashvili**: Investigation. **Hava Rosenfeld**: Methodology. **Dan Scharf**: Software. **Keren Shichrur**: Methodology. **Elena Shinderman-Maman**: Investigation. **Sarah Elitzur**: Resources. **Yehudit Birger**: Resources. **Shai Izraeli**: Conceptualization; supervision; funding acquisition; writing—review and editing. **Yosef E Maruvka**: Conceptualization; funding acquisition; supervision; writing—review and editing.

CONFLICT OF INTEREST STATEMENT

The authors declare no conflict of interest.

DATA AVAILABILITY STATEMENT

The data that support the findings of this study are openly available in the EMBL/EBI European Nucleotide Archive at https://www.ebi.ac.uk/, reference number REQ20250826212709.

DNA sequence data have been archived at the EMBL/EBI European Nucleotide Archive under accession number REQ. 20 250 826 212 709.

ETHICS STATEMENT

The study was conducted in accordance with the Declaration of Helsinki, under approval of the institutional review board of Rabin Medical Center, and was carried out according to local guidelines and regulations.

FUNDING

This research was supported by the Israeli Science Foundation (ISF) grants number 2794/21 (YEM) and personalized medicine program grant No. 3120/22 (SI, YEM), the Israel Cancer Research Foundation Professorship grant (SI), Fight Kids Cancer Foundation (SI), the Nevzlin Foundation (SI, YB, and RS), the Varda and Boaz Dotan Center, and the Shapiro chair for hematological malignancies at Tel Aviv University (SI). SE was supported by a grant from the Boxenbaum Foundation, awarded through the Israel Cancer Association.

SUPPORTING INFORMATION

Additional supporting information can be found in the online version of this article.

ORCID

Ruth Shiloh https://orcid.org/0009-0006-3646-4749
Dana Dayan https://orcid.org/0009-0002-0628-7893
Jorge Cano-Nistal https://orcid.org/0000-0002-3570-322X
Shlomit Barzilai-Birenboim https://orcid.org/0000-0002-3994-0556
Jamal Mahajna https://orcid.org/0000-0003-2218-2039
Nino Oniashvili https://orcid.org/0009-0002-7424-473X
Keren Shichrur https://orcid.org/0009-0001-1600-9312
Sarah Elitzur https://orcid.org/0000-0002-3495-7578
Shai Izraeli https://orcid.org/0009-0001-2131-8638
Yosef E. Maruvka https://orcid.org/0000-0002-8918-9887

REFERENCES

1. Zwaan CM, Tasian SK, Aplenc R, et al. Diagnosis and management of aml in pediatric patients: consensus recommendations from an international expert panel. *Blood*. 2026;147(14):1532-1561.
2. Cloos J, Valk PJM, Thiede C, et al. 2025 Update on MRD in acute myeloid leukemia: a consensus document from the ELN-DAVID MRD working party. *Blood*. 2026;147(11):1147-1167.
3. Bolouri H, Farrar JE, Triche, Jr. T, et al. The molecular landscape of pediatric acute myeloid leukemia reveals recurrent structural alterations and age-specific mutational interactions. *Nat Med*. 2018; 24(1):103-112.
4. Umeda M, Ma J, Westover T, et al. A new genomic framework to categorize pediatric acute myeloid leukemia. *Nat Genet*. 2024;56(2): 281-293.
5. Tierens A, Bjørklund E, Siitonen S, et al. Residual disease detected by flow cytometry is an independent predictor of survival in childhood acute myeloid leukaemia; results of the NOPHO-AML 2004 study. *Br J Haematol*. 2016;174(4):600-609.
6. Buldini B, Maurer-Granofszky M, Varotto E, Dworzak MN. Flow-cytometric monitoring of minimal residual disease in pediatric patients with acute myeloid leukemia: recent advances and future strategies. *Front Pediatr*. 2019;7:412.
7. Juul-Dam KL, Ommen HB, Nyvold CG, et al. Measurable residual disease assessment by qPCR in peripheral blood is an informative tool for disease surveillance in childhood acute myeloid leukaemia. *Br J Haematol*. 2020;190(2):198-208.
8. Scott S, Devonshire A, Dillon R, et al. Recommendations from the AML molecular MRD expert advisory board. *Leukemia*. 2024;38(7): 1638-1641.
9. Jongen-Lavrencic M, Grob T, Hanekamp D, et al. Molecular minimal residual disease in acute myeloid leukemia. *N Engl J Med*. 2018; 378(13):1189-1199.
10. Bachas C, Schuurhuis GJ, Hollink IHIM, et al. High-frequency type I/II mutational shifts between diagnosis and relapse are associated

with outcome in pediatric AML: implications for personalized medicine. *Blood*. 2010;116(15):2752-2758.
11. Farrar JE, Schuback HL, Ries RE, et al. Genomic profiling of pediatric acute myeloid leukemia reveals a changing mutational landscape from disease diagnosis to relapse. *Cancer Res*. 2016;76(8):2197-2205.
12. Zaliova M, Zuna J, Winkowska L, et al. Genomic DNA-based measurable residual disease monitoring in pediatric acute myeloid leukemia: unselected consecutive cohort study. *Leukemia*. 2024;38(1):21-30.
13. van der Velden VHJ, Dombrink I, Alten J, et al. Analysis of measurable residual disease by IG/TR gene rearrangements: quality assurance and updated EuroMRD guidelines. *Leukemia*. 2024;38(6):1315-1322.
14. Gröbner SN, Worst BC, Weischenfeldt J, et al. The landscape of genomic alterations across childhood cancers. *Nature*. 2018; 555(7696):321-327.
15. Duployez N, Marceau-Renaut A, Boissel N, et al. Comprehensive mutational profiling of core binding factor acute myeloid leukemia. *Blood*. 2016;127(20):2451-2459.
16. Ma X, Liu Y, Liu Y, et al. Pan-cancer genome and transcriptome analyses of 1,699 paediatric leukaemias and solid tumours. *Nature*. 2018;555(7696):371-376.
17. Miles LA, Bowman RL, Merlinsky TR, et al. Single-cell mutation analysis of clonal evolution in myeloid malignancies. *Nature*. 2020; 587(7834):477-482.
18. Herlin MK, Yones SA, Kjeldsen E, Holmfeldt L, Hasle H. What is abnormal in normal karyotype acute myeloid leukemia in children? Analysis of the mutational landscape and prognosis of the TARGET-AML Cohort. *Genes*. 2021;12(6):792.
19. Ruff DW, Dhingra DM, Thompson K, Marin JA, Ooi AT. High-throughput multimodal single-cell targeted dna and surface protein analysis using the mission bio tapestri platform. *Methods Mol Biol*. 2022;2386:171-188.
20. Karol SE, Coustan-Smith E, Pounds S, et al. Clinical impact of minimal residual disease in blood and bone marrow of children with acute myeloid leukemia. *Blood Adv*. 2023;7(14):3651-3657.
21. Bonnet D, Dick JE. Human acute myeloid leukemia is organized as a hierarchy that originates from a primitive hematopoietic cell. *Nat Med*. 1997;3(7):730-737.
22. Sarry JE, Murphy K, Perry R, et al. Human acute myelogenous leukemia stem cells are rare and heterogeneous when assayed in NOD/SCID/IL2Rγc-deficient mice. *J Clin Invest*. 2011;121(1): 384-395.
23. Quek L, Otto GW, Garnett C, et al. Genetically distinct leukemic stem cells in human CD34- acute myeloid leukemia are arrested at a hemopoietic precursor-like stage. *J Exp Med*. 2016;213(8): 1513-1535.
24. Malmberg EBR, Ståhlman S, Rehammar A, et al. Patient-tailored analysis of minimal residual disease in acute myeloid leukemia using next-generation sequencing. *Eur J Haematol*. 2017;98(1):26-37.
25. Delsing Malmberg E, Rehammar A, Pereira MB, et al. Accurate and sensitive analysis of minimal residual disease in acute myeloid leukemia using deep sequencing of single nucleotide variations. *J Mol Diagn*. 2019;21(1):149-162.
26. van Putten J, Snaebjornsson P, Bosch LJW, et al. Real-world clinical utility of tumor whole-genome sequencing in solid cancers. *Nat Med*. 2026;32:1286-1295.
27. Tanaka T, Morita K, Loghavi S, et al. Clonal dynamics and clinical implications of postremission clonal hematopoiesis in acute myeloid leukemia. *Blood*. 2021;138(18):1733-1739.